

Swimming Efficiency of Bacterium Escherichia Coli

Suddhashil Chattopadhyay¹, Radu Moldovan¹, Chuck Yeung², and X.L. Wu^{1*}

¹Department of Physics and Astronomy, University of Pittsburgh, Pittsburgh, PA 15260 and
²School of Science, Pennsylvania State University at Erie, The Behrend College, Erie, PA 16563
(Dated: Dec 22, 2005)

We use measurements of swimming bacteria in an optical trap to determine fundamental properties of bacterial propulsion. In particular, we determine the propulsion matrix, which relates the angular velocity of the flagellum to the torques and forces propelling the bacterium. From the propulsion matrix, dynamical properties such as forces, torques, swimming speed and power can be obtained by measuring the angular velocity of the motor. We find significant heterogeneities among different individuals even though all bacteria started from a single colony. The propulsive efficiency, defined as the ratio of the propulsive power output to the rotary power input provided by the motors, is found to be 0.2%.

Bacteria swim by rotating helical propellers called flagella. In the case of *Escherichia coli* (*E. coli*), each flagellum is several microns in length, 20 nm in diameter and four to five of them organize into a bundle. The flagella are driven at their bases by reversible rotary engines that turn at a frequency of approximately 100 Hz. Existing experiments show that these molecular engines are Poisson stepping motors consisting of several hundred steps per revolution [1, 2]. However many essential properties of bacterial swimming have not been measured, particularly in intact cells. For example, what is the relation between the angular velocity of the propellers and the force propelling the bacteria forward? What fraction of the flagellar motor power is converted into translational motion? What variability is there in the swimming apparatus from cell to cell? Some of these fundamental questions have been addressed in theoretical and numerical work [3, 4, 5], however, direct measurements of intact cells with functional motors and flagella are limited [6, 7, 8].

Herein, we report an investigation of the fundamental swimming properties of *E. coli* using optical tweezers and an imposed external flow. We measure the force required to hold the bacterium, and the angular velocities of the flagellar bundle and of the cell body as a function of the flow velocity. The propulsion matrix, which relates the translational and angular velocity of the flagella to the forces and torques propelling the bacterium, can thus be determined one bacterium at a time. Our measurements show that although the population averaged matrix elements are in reasonably good agreement with the resistive force theory for helical propellers [4], there is a large variability among bacteria from a single colony. The propulsion matrix also allows us to determine the propulsive efficiency ε , defined as the ratio of the propulsive power output to the rotary power input, to be 0.2%. This is consistent with experiments on helical propellers [9] and close to the maximum efficiency for the given cell-body and shape of the flagella. It is

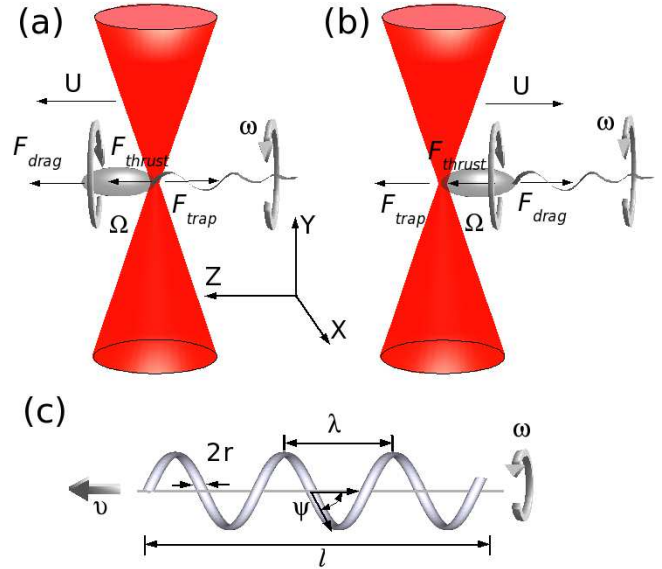


FIG. 1: Two different trapping configurations are possible. (a) The bacterium can be trapped at the tail of the cell body in the presence of an imposed flow U . The trapping is stable for $U \geq 0$. (b) The bacterium can also be trapped at the head of the cell body for U between $-40 \mu\text{m/s}$ and $-100 \mu\text{m/s}$. The forces and velocities are positive if they are along $+Z$. The rotations are defined by the right-hand rule such that $\omega < 0$ and $\Omega > 0$ as depicted. (c) A schematic of a helical flagellum: l is the length, $2r$ is the diameter of the filament, Ψ is the pitch angle of the helix relative to the swimming axis, and λ is the pitch.

smaller than the 1 or 2% predicted theoretically for simple shapes such as a corkscrew [5]. Our experimental technique is versatile and can be used to make comparative studies of mutant strains of the same species or of different micro-organisms. Such measurements can shed new light on how this remarkable ability to swim evolves among different bacterial species.

An important feature of bacterial swimming is that at very low Reynolds numbers ($Re \simeq 10^{-4}$), the fluid motion is governed by Stokes flow and nonlinearities in the full hydrodynamic equation are irrelevant. Despite this simplifying feature, the problem remains theoretic-

*Electronic address: xlwu@pitt.edu

cally difficult due to complicated time-dependent boundary conditions. Theoretical studies, therefore, usually assume that the flagella have very simple geometries such as an infinite sheet [3] or a helical coil [4, 5]. A second approach is not to take into account specific geometries but to consider general relations appropriate in the low Reynolds number limit [9]. In this regime, the torque N_{fl} acting on the propeller and the thrust force F_{thrust} generated by the propeller are linearly related to the propeller's angular velocity ω and the translational velocity v (relative to the background fluid):

$$-F_{thrust} = Av - B\omega \quad (1a)$$

$$N_{fl} = -Bv + D\omega. \quad (1b)$$

The above equation can be expressed in terms of the symmetric propulsion matrix $P = \begin{bmatrix} A & -B \\ -B & D \end{bmatrix}$, also known as the resistance matrix [10]. Choosing the coordinate system in Fig. 1, F_{thrust} and v are positive if directed toward the head of the cell while the sign of ω and N_{fl} obeys the right-hand rule, i.e., the flagella is a left-handed helix. Based on this coordinate system, the coefficients A , B , and D are positive, proportional to fluid viscosity η , and depend on the shape and size of the propeller. The basic physics is that in the absence of an applied torque, a translating propeller under the influence of an external force must rotate, and in the absence of an applied force, a rotating propeller under the influence of an external torque must translate [9]. The above formulation is applicable to propellers of any shape and size. However, for the special case of a helical coil, the matrix elements can be derived from resistive force theory [4]:

$$A = K_n \ell \frac{(1 - \beta(1 - \gamma_k))}{\beta^{1/2}}, \quad (2a)$$

$$B = K_n \ell \frac{\lambda(1 - \beta)(1 - \gamma_k)}{2\pi\beta^{1/2}}, \quad (2b)$$

$$D = K_n \ell \frac{\lambda^2(1 - \beta)}{4\pi^2\beta^{1/2}} \left(1 + \gamma_k \frac{(1 - \beta)}{\beta} \right), \quad (2c)$$

where ℓ is the length of the coil, and $\beta = \cos^2 \Psi$ with Ψ being the pitch angle relative to the swimming axis (see Fig. 1c). The quantity γ_k is the ratio of the tangential viscous coefficient $K_t = 4\pi\eta/(2\ln(0.18\lambda/r) - 1)$ to the perpendicular viscous coefficient $K_n = 8\pi\eta/(2\ln(0.18\lambda/r) + 1)$, where λ is the pitch and r is the radius of the coil filament. For a smooth coil, Lighthill [4] predicts that $\gamma_k = K_t/K_n \approx 0.7$. As can be seen, the helix loses its ability to propel, if $\gamma_k \rightarrow 1$, $\Psi \rightarrow 0$ ($\beta \rightarrow 1$) or $\Psi \rightarrow \frac{\pi}{2}$ ($\lambda \rightarrow 0$) as expected.

To complete the model of the swimming bacterium, we need the propulsion matrix P_0 for the cell body. Unlike P for the flagellum, P_0 is diagonal ($B_0 = 0$) since the cell body cannot propel itself. The non-viscous force on the cell body consists of two parts, the trapping force F_{trap} due to the optical tweezer holding the bacteria and the thrust F_{thrust} generated by the flagella. The sum of

these forces should balance the viscous force $A_0 v$ acting on the cell body. Likewise, the non-viscous torque acting on the cell body $-N_{fl}$ should be balanced by the viscous rotational drag. This gives:

$$F_{trap} + F_{thrust} = A_0 v, \quad (3a)$$

$$D_0 \Omega = -N_{fl}, \quad (3b)$$

where Ω is the angular velocity of the cell body. We treat the cell body as a prolate with minor semi-axis a and major semi-axis b so that the linear and rotational drag coefficients are $A_0 = 4\pi\eta b/(\ln(\frac{2b}{a}) - \frac{1}{2})$ and $D_0 = 16\pi\eta a^2 b/3$ [11]. The optical trapping force is harmonic $F_{trap}(z) = -k(z - z_0)$, where k is the spring constant and $z - z_0$ is the displacement from the center of the trap [12, 13]. Since the bacteria held by the optical tweezer, its net velocity in the lab frame is zero ($v' = v + U \simeq 0$), and the relative velocity v is opposite to the external flow U . Substituting $v = -U$ into Eqs. 1 and 3 gives:

$$k(z - z_0) = (A + A_0)U + B\omega, \quad (4a)$$

$$D_0 \Omega = -BU - D\omega. \quad (4b)$$

This set of equations will be used below to analyze our data.

We used a non-tumbling strain of bacteria (RP5231) in our measurements. We were delighted to find that such a bacterium swimming a few microns above a glass surface could be stably trapped, along its swimming direction, by the optical tweezer [14]. The bacterium can then be manipulated by an imposed external flow. Figure 1 illustrates our experimental setup along with the flow configurations. A bacterium swimming to the left (along the $+Z$ direction) is held by a strongly focused IR laser ($\lambda = 1024 \text{ nm}$). In the absence of the flow, the bacterium is invariantly held by the tail of the body. The thrust force and the trapping force are balanced and the bacterium is stationary with respect to the trap. The trapping remains stable when a uniform flow in the $+Z$ direction is applied ($U > 0$) [15]. The bacterium can also be trapped at the head of the body, but the flow field must be reversed ($U < 0$).

To measure the trapping force and the position of the trapped cell tip, the transmitted IR beam was refocused by a high numerical aperture condenser (N.A. 1.5) and projected onto a two-dimensional position sensitive detector (Pacific Silicon Sensor Inc., DL100-7PCBA). The position of the trapped cell tip with respect to the center of the trap is monitored by a PC equipped with a National Instruments analog-digital converter card (AT-MIO-16E-2). The conversion rate is 10 kHz at 12-bit resolution. A non-flagellated bacterium was used to calibrate the spring constant k of the optical trap by measuring the position of the trapped tip as a function of the flow U . For the laser intensity (23 mW) used in this experiment, $k = 5.7 \times 10^{-6} \text{ N/m}$. A brief description of the calibration process is presented in Materials and Methods.

Figure 2 displays an example of the time trace $z(t)$, the longitudinal displacement along the swimming direction

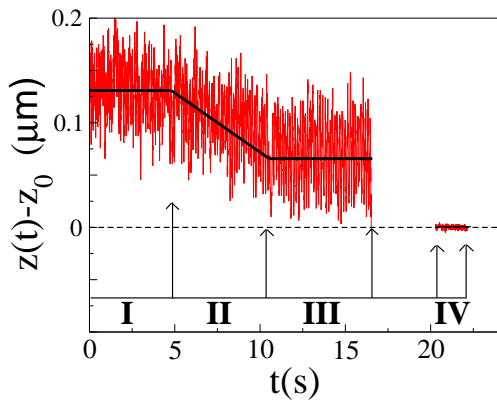


FIG. 2: A typical experimental run for a swimming bacterium held in the optical trap. An uniform flow $U = 10 \mu\text{m/s}$ is established in regime I. The flow U is decreased to zero linearly in regime II. The flow U remains zero in regime III. The laser is switched off momentarily to let the bacterium escape and the undeflected laser beam position is recorded in regime IV. Solid lines depict linear fits to each regimes.

of a trapped bacterium. We observed large oscillations overlying a systematic variation of $z(t)$ as the external flow is changed. These oscillations result from wobbling of the cell body in response to the rotation of the flagella bundle [16, 17]. The trapped bacterium was perturbed by the following sequence of events: In regime I, the bacterium is subject to a uniform flow $U = +10 \mu\text{m/s}$. The bacterium maintains an average position away from the center of the trap. In regime II, U is linearly reduced to zero in 5 s. The average bacterium position shifts systematically toward the center of the trap. In regime III, U is maintained at zero for 5 s, and the average position of the bacterium relative to the trap is again constant. Finally in regime IV, the bacterium is released. The position of the undeflected beam in regime IV is taken to be z_o , the center of the optical trap. From regime II we obtain the net translational drag coefficient $A + A_0 = k\Delta z/\Delta U$, and in regime III we obtain F_{thrust} , since $F_{trap} = F_{thrust}$ when $U = 0$. We checked that this measurement was reproducible by returning the flow to $U = 10 \mu\text{m/s}$ rather than releasing the bacterium after regime III. The bacterium returned to within a few percent of its initial average position.

We extracted the angular velocities Ω and ω using a Fourier analysis of the time trace $x(t)$ of the transverse position of the cell body. This transverse signal shows more pronounced oscillations than $z(t)$. Figure 3(a) displays a sample power spectrum $E(f)$ for a short time trace of 5 s when $U = 0$ (regime III). The power spectrum has two strong peaks at $f_L \simeq 7 \text{ Hz}$ and $f_H \simeq 130 \text{ Hz}$, respectively. These two frequencies can be associated with the angular velocities of the cell-body $\Omega = 2\pi f_L$ and of the flagellum bundle $\omega = -2\pi f_H$ [16]. Averaging over 250 bacteria, we found $\bar{f}_L = (8.0 \pm 0.2) \text{ Hz}$ and $\bar{f}_H = (125 \pm 2) \text{ Hz}$, where the \pm are standard errors of the mean. However, as shown in Fig. 3(c-d) there

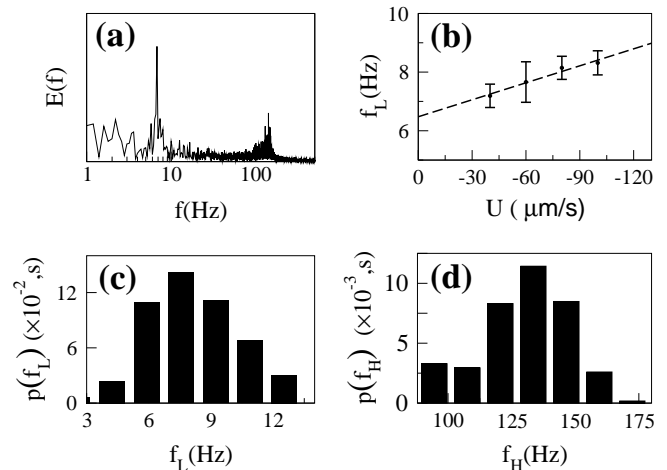


FIG. 3: (a) Power spectrum of $x(t)$ shows peaks corresponding to f_L and f_H . (b) The variation of the rotation frequency of the cell body f_L as a function of flow speed U . The linear dependence is consistent with the propulsion matrix formulation. (c) and (d) delineate the PDFs of f_L and f_H , respectively. Error bars are standard errors of the mean unless otherwise noted.

is considerable variation of f_L and f_H between individual bacteria. The standard deviations $\sigma_{f_L} = 2.4 \text{ Hz}$ and $\sigma_{f_H} = 27 \text{ Hz}$ are respectively 20 and 30 % in the mean values.

To test the basic physics implied by the propulsion matrix, we measured the dependence of f_L and f_H on U for an additional 40 bacteria which were subjected to flow speeds of $U = -40, -60, -80$ and $-100 \mu\text{m/s}$. Figure 3(b) shows that the average frequency \bar{f}_L increases linearly with $-U$ and the result is in good agreement with Eq. 4b, as predicted by the propulsion matrix formulation. Within the noise of the measurement, no systematic change in \bar{f}_H was detected. This is expected since at low-loads the molecular motor is known to rotate at a constant angular speed independent of the load [18].

To complete our determination of the propulsion matrix, the semi-minor axis a and length $L_{cell} = 2b$ of the bacteria were measured directly by video microscopy while immobilized in the trap. This allows us to calculate the drag coefficients A_0 and B_0 for the cell body. From the time trace $z(t)$, A and B are calculated by $A = k\Delta z/\Delta U - A_0$ and $B = F_{thrust}/\omega$ when $U = 0$. Finally, the measurements of the angular velocities gives $D = -D_0\omega/\Omega$. The matrix elements averaged over a population of 250 bacteria are $\bar{A} = (3.8 \pm 0.2) \times 10^{-8} \text{ N s/m}$, $\bar{B} = (4.0 \pm 0.1) \times 10^{-16} \text{ N s}$, and $\bar{D} = (5.9 \pm 0.1) \times 10^{-22} \text{ N s m}$. The translational drag coefficient of the flagella is approximately twice that of the cell body ($A_0 = 1.7 \times 10^{-8} \text{ N s/m}$). Therefore a significant portion of drag is due to the flagella. On the other hand, the rotational drag of the flagella \bar{D} is much smaller than that of the cell body ($\bar{D}_0 = 8.8 \times 10^{-21} \text{ N s m}$).

It is instructive to use the measured propulsion matrix to extract physical parameters that are relevant to flag-

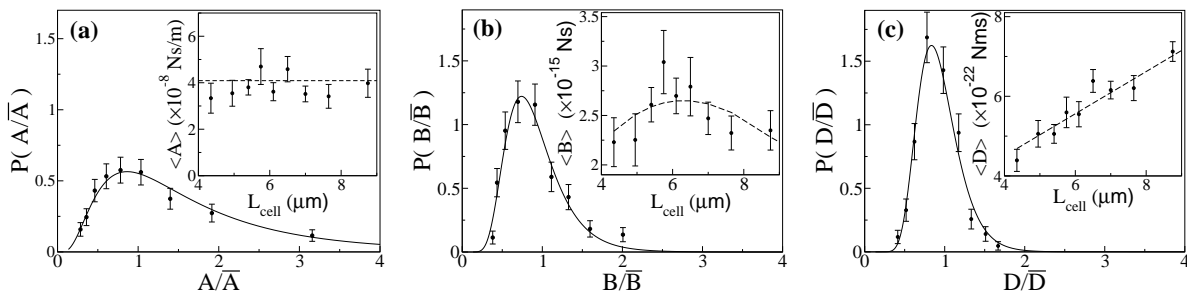


FIG. 4: The PDFs of (a) A/\bar{A} , (b) B/\bar{B} , and (c) D/\bar{D} . The insets show the length L_{cell} dependence of (a) $\langle A \rangle$, (b) $\langle B \rangle$, and (c) $\langle D \rangle$. The solid lines in the main figures are fits to log-normal distributions.

ellar bundles. The resistive force theory for the helix coil contains four independent parameters: the pitch λ , the pitch angle Ψ , the length of the helix ℓ , and the radius r of the filament, assuming that the viscosity of the fluid ($\eta = 10^{-3} Pa s$) is known. The three matrix elements A , B , and D in Eqs. 2 however are not sufficient to predict all the four geometric parameters. To make progress, we assumed that the pitch angle Ψ is 41° , as determined by Turner et al. using fluorescently labeled *E. coli* cells [7]. This angle also turns out to be remarkably close to the optimal angle (42°) that maximizes the propulsion efficiency of an ideal helix [4]. Using $\beta = \cos^2(41^\circ) = 0.57$, Eqs. 2 predict $\gamma_k = 0.84$, $\lambda = 0.9 \mu m$, $r = 23 nm$, and $\ell = 6.2 \mu m$. These values are comparable to the fluorescent measurements of Turner et al. who found $\bar{\ell} = 7 \mu m$, and $\bar{\lambda} \approx 1 \mu m$ for the curly flagella and $2.2 \mu m$ for the normal ones [7]. We can estimate the average number of flagella using $r \approx \sqrt{N} r_o$, which gives $\bar{N} \approx r^2/r_o^2 \approx 5.3$. This is slightly greater than the $\bar{N} \approx 3.3$ found by Turner et al. The difference may be expected because the bacteria used in their experiment are shorter than the ones we studied; longer bacteria usually have more flagella.

All important dynamical quantities can be obtained from our measurements. For example, the average thrust for $U = 0$ is $\bar{F}_{thrust} = \bar{B} \bar{\omega} = 0.31 pN$. The average swimming speed is $\bar{V}_{swim} = \bar{B} \bar{\omega} / (\bar{A}_0 + \bar{A}) = 6 \mu m/s$, which should be compared with $V_{swim} \approx 10 \mu m/s$ we obtained directly by video microscopy. The difference may be due to correlations between A , B and D ; both B and D grows with A on average. Similarly the average torque $\bar{N}_{fl} = \bar{D} (|\bar{\omega} - \bar{\Omega}|) = 4.9 \times 10^{-19} N m$ is surprisingly close to that found for *Streptococcus* [18].

We observed that the propulsion matrix elements vary greatly among individual bacteria even though our bacteria are from a single colony. Figure 4 shows the probability distribution functions (PDF) of the scaled quantities A/\bar{A} , B/\bar{B} , and D/\bar{D} . The standard deviations σ are comparable to the mean values with $\sigma_A/\bar{A} = 0.7$, $\sigma_B/\bar{B} = 0.5$ and $\sigma_D/\bar{D} = 0.3$. A conspicuous feature of all the PDFs is their broad tails, particularly for the linear drag coefficient A . This might be an indication of either significant structural heterogeneities in the flagellar bundles of individual cells or of changes in conformations of the flagellar bundle with time. As is often the case in

biological systems, the PDFs can be roughly fitted to log-normal distribution functions, which are plotted as solid lines in the figure.

Part of the variation in A , B and D must arise due to bacteria being in different stages of their growth cycle during the measurements. This is particularly the case in the middle log-phase of a growing culture, where the bacterial size is highly varied. For ease of trapping, very long and very short bacteria were excluded from the measurements and the middle-sized bacteria ($4 - 12 \mu m$), which comprised about 95% of the population, was chosen. The bacterial cell-length distribution of this selected population is plotted in Fig. 5(a). The figure also shows the cell length at which we first observed septal rings (dotted line) and the length at which cells divide (solid line). We used the bacterial length L_{cell} as a measure of the bacterium's physiological state and determine the propulsive matrix elements as a function of L_{cell} . To determine the length dependence of the coefficients A , B , and D , we calculated the averaged values $\langle A \rangle$, $\langle B \rangle$ and $\langle D \rangle$ for bacteria of similar length. The result are presented in the insets of Fig. 4(a-c). The linear drag coefficient $\langle A \rangle$ has no clear size dependence but $\langle B \rangle$ is peaked at $L_{cell} \approx 6 \mu m$, which coincides with the peak of the size distribution. On the other hand, Fig. 4(c) shows that the rotational drag coefficient $\langle D \rangle$ of the propeller grows linearly with the cell-body length L_{cell} .

These size dependencies allow us to draw conclusions about the structure of flagellar bundles at different stages of cell growth. Inspection of Eqs. 2 shows that the matrix elements scale with the pitch λ according to $A \propto \lambda^0$, $B \propto \lambda^1$, and $D \propto \lambda^2$. The fact that we find that B and D depend on L_{cell} but A does not, implies that the primary L_{cell} dependence is in pitch λ . The pitch angle Ψ and the flagella length ℓ are approximately constant independent of L_{cell} . Likewise, γ_k depends logarithmically on λ and so is only very weakly dependent on L_{cell} . Since our measurements show a linear relation between D and L_{cell} , it suggests that λ^2 grows linearly with L_{cell} . A possible scenario for this is that more and more flagella are incorporated into the bundle as the bacteria cell body grows and this causes the λ^2 to grow in agreement with Fig. 4(c). From the shortest to the longest bacterial body size (L_{cell}), we found that the fractional change

$\delta\lambda/\lambda$ is about 16%, which may be discernible in carefully conducted observations using fluorescently labeled bacteria.

We next turn our attention to the power and propulsive efficiency of the swimming bacteria. The average power output of the flagellar motors is $\bar{\Sigma} = D_0\Omega(\omega - \Omega) = 0.4 \text{ pW}$. The power used to turn the cell body is $D_0\Omega^2 \approx 0.02 \text{ pW}$ while the actual propulsive power is another factor of ten smaller with $A_0V_{swim}^2 \approx 0.0017 \text{ pW}$. Therefore 5% of the rotary power is used to rotate the

cell body, and only 0.5% is used to push the bacteria forward. Figure 5(b) shows the average motor power as a function of bacterial length L_{cell} . The power increases gradually with L_{cell} , which is consistent with the above discussion that the number of flagella N and the associated motors increase with L_{cell} . The propulsion efficiency ε , defined as the ratio of the propulsive output power to the rotary input power, can be related to the propulsion matrix elements [9]:

$$\varepsilon \equiv \frac{A_0v^2}{N_{fl}(\omega - \Omega)} = \frac{A_0D_0B^2}{[(A_0 + A)D - B^2][(A_0 + A)(D_0 + D) - B^2]} \approx \frac{A_0B^2}{(A_0 + A)^2D} \quad (5)$$

Here we used $B^2 \ll (A_0 + A)D$ and $D_0 \gg D$ to obtain the approximate form. These assumptions are met on average but does not always hold for a particular bacterium. Therefore we use the full form to calculate the efficiency. Figure 5(c) shows that the efficiency as a function of bacterial size is constant up to the cell division length ($L_{cell} = 8 \text{ }\mu\text{m}$). The average efficiency $\bar{\varepsilon} \approx 0.2\%$ [19] is surprisingly close to that of sedimenting helices in a silicon oil, which were tested as model flagella by Purcell [9]. We can also ask, for a given A_0 , what is the maximum efficiency attainable by the bacterium as a function of the length of the flagella. Assume that at some characteristic length ℓ_p , the propulsive coefficients of the flagellum are A_p , B_p and D_p . Neglecting logarithmic corrections and assuming the width of the flagellar bundle is constant, these coefficients should grow linearly with flagella length ℓ so that $A \approx \kappa A_p$, $B \approx \kappa B_p$ and $D \approx \kappa D_p$ where $\kappa = \ell/\ell_p$. This assumption is consistent with Eqs. 2. Substituting for A , B and D into our approximate expression for ε (in Eq. 5) we find that the maximum efficiency occurs when $A = A_0$ and that $\varepsilon_{max} \approx B_p^2/(4A_pD_p)$ which depends only on the shape of the propeller. The same result was obtained by Purcell when he maximized ε by assuming that all propeller dimensions (not just the length) scaled with κ [9]. In our experiments, we find that $A \approx 2A_0$ and so flagella are twice as long as that required to maximize its propulsive efficiency. However, the peak in ε as a function of κ is fairly broad and the observed efficiency is about 75% of the maximum efficiency as shown by the solid and dashed lines in Fig. 5c. The broadness of the peak may be why the propulsive efficiency is approximately constant throughout the bacterial cell division cycle. The experimental propulsive efficiencies are consistent with the small ε_{max} of between 0.3% – 0.8% measured for helical propellers [9]. It is smaller still than the 1 or 2% predicted theoretically for a helical propeller [4, 5].

In summary, bacterial propulsion in a uniform stream is investigated with the help of optical tweezers, which allow the thrust force F_{thrust} to be directly measured as

a function of imposed flow. For a free swimming bacterium, F_{thrust} precisely balances the viscous drag of the cell body A_0v and of the flagellar bundle Av . The contribution to the drag by Av is twice as large as A_0v but is difficult to determine without our direct force measurements. We also showed that the propulsion matrix description proposed by Purcell gives an adequate description of bacterial propulsion over a physiological range of velocities. In retrospect, the validity of the propulsion matrix, or for that matter the resistive force theory itself, is not self evident for real micro-organisms because of possible deformations of flagellar bundles due to hydrodynamic stresses induced by swimming or by the flow [5].

We have determined all elements of the propulsion matrix and used the resistive force calculations for a helical coil to estimate microscopic properties of flagella [4]. The results were consistent with earlier measurements even though the resistive force calculations neglect the effect of long-range hydrodynamics interactions between different parts of the flagella and with the cell body. Using the propulsion matrix, we have determined all dynamic quantities related to bacterial swimming and their dependence on the size of the cell body. In particular, we found that the propulsive efficiency ε , defined as the ratio of the propulsive power output to the rotary power input, is $\sim 0.2\%$ and is nearly independent of L_{cell} . The measured ε is consistent with the experiments on rigid helical propellers [9] and close to the maximum efficiency for the given size of the cell body and the shape of the flagellar bundle. A conspicuous finding of our measurements is that all the matrix elements are broadly distributed despite the fact that all bacteria started from a single colony. The ubiquity of such broad distributions in biological systems is significant and begs further systematic study.

MATERIALS AND METHODS

Sample preparation: We followed standard growth con-

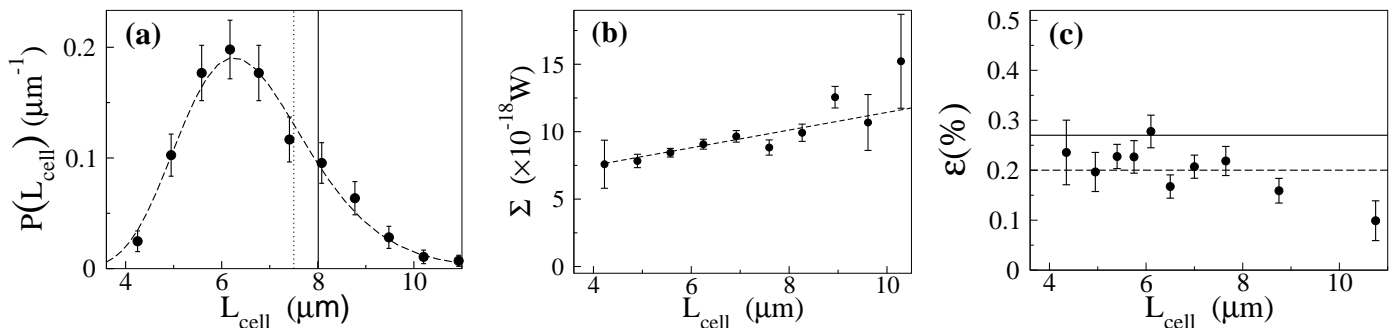


FIG. 5: (a) The PDF of the bacterial cell length L_{cell} . The dashed line is a fit to the log-normal distribution. The dotted and solid vertical lines are, respectively, the cell lengths at which we first observed a septal ring and where cell division occurred. (b) The flagellar power output $\langle \Sigma \rangle$ as a function of L_{cell} . The dashed line is a linear fit. (c) The propulsion efficiency $\langle \epsilon \rangle$ as a function of L_{cell} . The dotted horizontal line marks the mean efficiency 0.2% of the entire population. The solid horizontal line is the maximum efficiency $\bar{\epsilon}_{max}$ when the flagellum length is optimized. See text for details.

ditions for culturing bacteria *E. coli* strains, RP5231 and YK4516. RP5231 is a smooth swimming strain because two of its chemotactic genes, *CheY* and *CheZ*, were deleted. A single colony was picked from a fresh agar plate and grown to saturation overnight in the LB medium (peptone 4 g, yeast 2 g, NaCl 1 g, 1M NaOH 0.4 ml; for 400 ml of media). The culture was maintained at 30 °C and was shaken continuously at 200 rpm. The overnight sample was diluted 1:100 in fresh LB medium and grown to the middle log phase for 3 hours.

To calibrate the spring constant k of the optical trap, we used non-flagellated bacteria strain YK4516. A uniform flow U was applied and the shift in the

centroid of the transmitted IR laser beam was recorded by the position detector. For an ellipsoid body, the translational drag coefficient A_o is known and the spring constant is obtained using $k = A_o \Delta U / \Delta z$. The noise in the output of the optical trap was $0.1 \text{ nm} / \sqrt{\text{Hz}}$ (for $z_{rms} = 5.2 \text{ nm}$ and sampling rate 10 KHz).

ACKNOWLEDGEMENTS

We would like to thank Emily Chapman, Roger Hendrix, and Bob Duda for helpful discussions and technical assistance. This research is supported by the National Science Foundation under Grant no. DMR-0242284.

-
- [1] Samuel, A. D. T. & Berg, H. C. (1996) *Biophys. J.* **71**, 918–923.
- [2] Sowa, Y., Rowe, A. D., Leake, M. C., Yakushi, T., Homma, M., Ishijima, A., & Berry, R. M. (2005) *Nature* **437**, 916–919.
- [3] Taylor, G. I. (1952) *Proc. Roy. Soc. London A* **211**, 225–239.
- [4] Lighthill, J. (1989) *Mathematical Biofluidynamics*. (SIAM, Philadelphia), 3rd edition, pp. 45–92.
- [5] Childress, S. (1981) *Mechanics of swimming and flying*, Cambridge Studies in Mathematical Biology. (Cambridge University Press, New York), 1st edition, pp. 34–60.
- [6] Meister, M., Lowe, G., & Berg, H. C. (1987) *Cell* **49**, 643–650.
- [7] Turner, L., Ryu, W. M., & Berg, H. C. (2000) *J. Bacteriol.* **182**, 2793–2801.
- [8] Magariyama, Y., Sugiyama, S. & Kudo, S. (2001) *FEMS Microbiol. Lett.* **199**, 125–129.
- [9] Purcell, E. M. (1997) *Proc. Natl. Acad. Sci. USA* **9**, 11307–11311.
- [10] Happel, J. & Brenner, H. (1965) *Low Reynolds Number Hydrodynamics with Special Applications to Particulate Media*. (Prentice-Hall, Englewood Cliffs), 1st edition, pp. 173–183.
- [11] Berg, H. C. (1993) *Random Walks in Biology*. (Princeton University Press, New Jersey), 1st edition, pp. 57–84.
- [12] Wuite, G. J., Davenport, R. J., Rappaport, A., & Bustamante, C. (2000) *Biophys. J.* **79**, 1155–1167.
- [13] Neuman, K. & Block, S. (2004) *Rev. Sci. Instr.* **75**, 2787–2809.
- [14] We found that it was difficult to stably trap and measure the force on the bacteria, when it is swimming perpendicular to the optical trap, in the interior of the fluid. The presence of the surface may have some effect on our measurements but does not change our qualitative conclusions.
- [15] We introduced the uniform flow U by translating the sample chamber using a Newport DC motor controller (Model 855) and two motorized translation stages. By controlling the velocities of two oppositely moving stages, a broad range of U (from 0 to 100 $\mu\text{m/s}$) can be achieved.
- [16] Rowe, A. D., Leake M. C., Morgan, H., & Berry, R. M. (2003) *J. of Mod. Opt.* **50**, 1539–1554.
- [17] Lowe, G., Meister, M., & Berg, H. C. (1987) *Nature* **325**, 637–640.
- [18] Chen, X. & Berg, H. C. (2000) *Biophys. J.* **78**, 1036–1041.
- [19] Note that due to the correlation of A , B and D , substituting the average values \bar{A} , \bar{B} , \bar{D} into Eq. 5 only gives an efficiency of 0.16% instead of 0.2%.